Journal of Catalysis 257 (2008) 190–198

Contents lists available at ScienceDirect

Journal of Catalysis

www.elsevier.com/locate/jcat

# Hydrochlorination of acetylene using supported bimetallic Au-based catalysts

Marco Conte [a], Albert F. Carley [a], Gary Attard [a], Andrew A. Herzing [b,c], Christopher J. Kiely [b], Graham J. Hutchings [a,*]

[a] School of Chemistry, Cardiff University, P.O. Box 912, Cardiff, CF10 3AT, UK
[b] Department of Materials Science and Engineering, Lehigh University, 5 East Packer Avenue, Bethlehem, PA 18015-3195, USA
[c] National Institute of Standards and Technology, Surface and Microanalysis Science Division, 100 Bureau Drive, Mailstop 8371, Gaithersburg, MD 20899-8371, USA

ARTICLE INFO

*Article history:*
Received 10 November 2007
Revised 24 April 2008
Accepted 26 April 2008
Available online 27 May 2008

*Keywords:*
Gold catalysis
Acetylene hydrochlorination
Supported bimetallic catalysts
Gold alloy nanoparticles

ABSTRACT

A detailed study of the hydrochlorination of acetylene using supported gold and gold-based bimetallic catalysts is described and discussed. Carbon-supported Au–Pd catalysts were studied in detail, because Au and Pd can form a continuous solid solution across all alloy compositions. The addition of $\leqslant$5 at% Pd to Au increased the initial activity but with a significant loss of selectivity. In addition, all Au–Pd/C catalysts deactivated rapidly due to coke deposition. Pt–Au catalysts behaved in a similar manner. In contrast, Au-catalysts doped with Ir and Rh demonstrated enhanced activity with little change in selectivity. The addition of Ru had no significant effect. The observations are rationalized in terms (i) of the relative solubilities of the second metal in Au, which were explored by detailed STEM–XEDS analysis, and (ii) the dehydrochlorination and oligomerization activity of the dopant metal. These results confirm that the most active known catalyst for the hydrochlorination of acetylene for long-term use is undoped Au, and that the activity of the catalyst correlates with the standard electrode potential.



## 1. Introduction

In previous work [1–6], we have shown that supported gold catalysts can be the materials of choice for the hydrochlorination of acetylene in the production of vinyl chloride monomer (VCM). The initial discovery that $Au^{3+}$ was the best catalyst for acetylene hydrochlorination [1] was based on an observation that the catalyst activity for a set of more than 30 carbon-supported metal chlorides correlated with the standard electrode potential of the cations. This correlation was rationalized based on the fact that most of the cations in the original study were divalent and that the interaction of the cation with acetylene involves a two-electron process. We subsequently demonstrated experimentally that gold was indeed the best catalyst for this reaction [2,3]. We also demonstrated, using $^{197}$Au Mössbauer spectroscopy [4], that the gold catalysts were deactivated by reduction of $Au^{3+}$ and that the catalysts could be reactivated by reoxidation using aqua regia [4] and $Cl_2$ or NO [5]. In particular, we found that the gold catalysts could be reactivated in situ using a co-feed of NO and that this did not change the selectivity and maintained high activity [5]. We subsequently studied the mechanism in more detail [6] and found that initial treatment with $C_2H_2$ led to lower activity, whereas pretreatment with HCl enhanced the initial activity. All of the current evidence that we have obtained for acetylene hydrochlorination using gold catalysts indicates that the active species is $Au^{3+}$. We consider that these active sites may be individual cations or gold cations on the surface of gold nanoparticles, perhaps at the interface with the carbon support. The charge-balancing anions most likely will be chloride, which in the fresh catalyst are retained from the chloroauric acid used in the preparation. During use, the catalyst surface will remain chlorided by the interaction with HCl.

Although largely superseded in many countries by processes based on ethene, the hydrochlorination of acetylene is one method through which VCM can be manufactured on a commercial scale in locations where coal-based economies remain active. Indeed, with the current rise in energy costs, coal-base processes are increasingly becoming financially competitive, and thus the manufacture of vinyl chloride using acetylene hydrochlorination can be expected to remain an important production route. In particular, we have demonstrated that supported gold catalysts have superior activities and lifetimes compared with the industrially preferred catalyst, based on carbon-supported mercuric chloride [7,8]. At present, there is sustained interest in catalysis by gold, and the subject is now well established in both heterogeneously and homogeneously catalyzed reactions [9–12]. Recently, we have shown that supported Au–Pd alloys can be very efficient catalysts for the direct synthesis of hydrogen peroxide [13] and the oxidation of alcohols to aldehydes [14]. This has prompted us to consider whether bimetallic catalysts composed of gold and another metal could give improved performance in the acetylene hydrochlorination reaction. For example, it is possible that such bimetallic systems might be

* Corresponding author. Fax: +44 29 2087 4075.
*E-mail address:* hutch@cf.ac.uk (G.J. Hutchings).

0021-9517/$ – see front matter 
doi:10.1016/j.jcat.2008.04.024

able to enhance the dispersion of gold cations. In this paper, we describe the effect of the addition of Pd, Ir, Rh, Pt, and Ru to Au to create bimetallic catalysts for this reaction. The main impetus for this work is to determine whether the activity of gold can be promoted by the addition of a second metal.

## 2. Experimental

### 2.1. Catalyst preparation and characterization

The carbon-supported gold catalyst (1 wt% Au/C) was prepared using an incipient wetness impregnation technique with aqua regia as a solvent. The carbon (Aldrich, Darco, 12–20 mesh) was initially washed with dilute aqueous HCl (1 mol $L^{-1}$) at 70 °C for 5 h to remove Na, Fe, and Cu contaminants, which are poisons for the hydrochlorination reaction. The carbon was filtered, washed with distilled water (2 L $g^{-1}$), and then dried at 140 °C for 18 h. A solution of $HAuCl_4 \cdot xH_2O$ (Strem, 82 mg, assay 49.7%) in aqua regia (3.7 mL) was added dropwise to the acid-washed carbon (Aldrich, Darco 12–20 mesh, 4 g) under stirring. The product was then dried at 140 °C for 18 h and used as a catalyst. A similar method was used to prepare both monometallic and bimetallic catalysts using $PdCl_2$, $H_2PtCl_6$, $RhCl_3 \cdot 3H_2O$, $IrCl_3 \cdot 3H_2O$, and $RuCl_3 \cdot 3H_2O$ (Strem) as the "dopant" metal precursor. All of the bimetallic catalysts used in this study had 1 wt% metal loading in total; thus, it should be noted that there is a difference in the molar quantities of the metals used in the mixed-metal catalysts.

X-ray photoelectron spectroscopy (XPS) was performed with a VG EscaLab 220i spectrometer using a standard Al$K_\alpha$ X-ray source (300 W) with an analyzer pass energy of 20 eV. Binding energies are referenced to the C 1s binding energy of carbon, taken to be 284.7 eV. Temperature-programmed reduction (TPR) was carried out using a Micromeritics ASAP 2910 instrument, using 10% $H_2$ in argon as a reductant and a temperature ramp of 50 to 300 °C (ramp rate, 10 °C $min^{-1}$; flow, 50 mL $min^{-1}$; final temperature, 300 °C, held for 1 h). Atomic absorption spectroscopy (AAS) was performed with a Perkin–Elmer 2100 atomic absorption spectrometer using an air–acetylene flame. Samples for examination by transmission electron microscopy (TEM) were prepared by dispersing the catalyst powder in high-purity ethanol, then allowing a drop of the suspension to evaporate on a holey carbon film supported by a 300-mesh copper TEM grid. Bright-field and annular dark-field (ADF) imaging experiments were carried out using a JEOL 2200FX TEM and an FEI Titan 80–300 TEM/STEM equipped with CEOS spherical aberration corrector, respectively. Samples were then subjected to chemical microanalysis and ADF imaging in a VG Systems HB603 scanning transmission electron miscroscope operating at 300 kV equipped with a Nion $C_s$ corrector. The instrument was fitted with an Oxford Instruments INCA TEM 300 system for energy-dispersive X-ray (XEDS) spectrometry. Multivariate statistical analysis (MSA) using the MSAXESP v. 0.11 code [15] was used to reduce the effect of random noise and aid quantitative analysis of the STEM–XEDS spectrum images generated in this study. MSA is a specialized set of processing techniques for analyzing the spectrum image data cube as a whole and identifying its independently varying components, thus allowing a significant reduction in the inherent background signal from the processed data [16]. Watanabe and co-workers [17–19] have shown that the application of MSA to STEM–XEDS spectrum imaging can significantly improve the quality and interpretability of the acquired data.

### 2.2. Catalyst testing

Catalysts were tested for acetylene hydrochlorination in a fixed-bed glass microreactor operating just above atmospheric pressure.

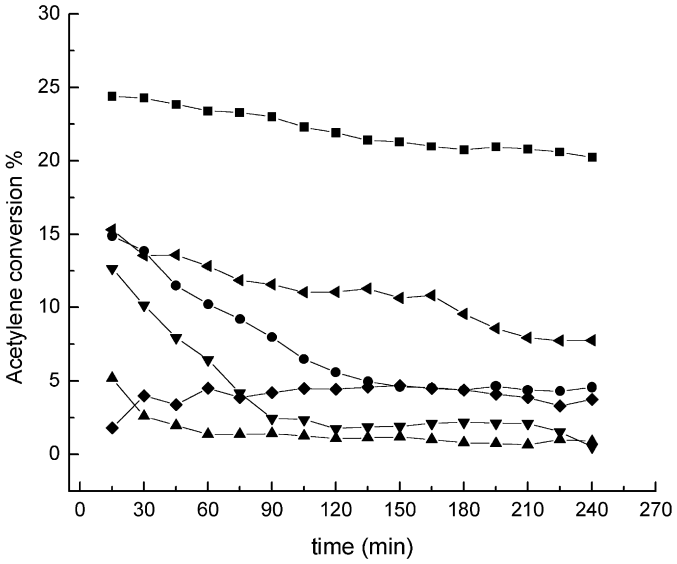


**Fig. 1.** Acetylene conversion using metal chlorinated salts of (■) Au, (▼) Pd, (◆) Pt, (▲) Rh, (●) Ir, and (◄) Ru on carbon as catalyst under standard reaction conditions ($C_2H_2$ and HCl 1:1 ratio; total flowrate 10 mL $min^{-1}$; catalyst (200 mg); 180 °C).

Acetylene (5 mL $min^{-1}$) and hydrogen chloride (5 mL $min^{-1}$) were fed though a mixing vessel/pre-heater (70 °C) via calibrated mass flow controllers to a heated glass reactor containing 200 mg of catalyst, giving a total GHSV of 870 $h^{-1}$. The pressure of the reactants, both HCl and $C_2H_2$, was in the range of 1.1–1.2 bar. This pressure level was chosen both for safety reasons and to test the catalyst under mild conditions. The products were analyzed in two ways. First, the exit gas mixture was passed through a Dreschel bottle containing NaOH at known concentration for a specified time to determine the conversion of HCl. Alternatively, the gas stream was analyzed by gas chromatography (GC). A reaction temperature of 180 °C was chosen, and blank tests using an empty reactor filled with quartz wool did not exhibit any catalytic activity with the reactants under these flow conditions, even at 250 °C. It should be noted that minor variability was found in experimental conversion values; however, different batches of Au/C catalysts were prepared and evaluated in triplicate, and the variation in the average data sets was insignificant (see Fig. S1 in Supplementary material). However, to make a fair comparison between Au/C and other catalysts, an Au/C catalyst was tested before each series of reactions, hence there are some small variations in the data that we report for the Au/C catalysts, but we have used this approach to ensure that we are able to delineate differences in the bimetallic catalysts and the standard Au/C catalyst.

## 3. Results and discussion

### 3.1. Activity of platinum group metals

The catalytic performance of a range of carbon-supported platinum group metals composed of equimolar amounts of metal (standardized to 1 wt% Au, confirmed by AAS) for the hydrochlorination of acetylene under standard reaction conditions ($C_2H_2$ and HCl 1:1 ratio; total flow rate 10 mL $min^{-1}$; 200 mg of catalyst; 180 °C) was investigated. The results (Fig. 1) show, as expected [1–5] that the Au/C catalyst gave the highest conversion of acetylene, with the following order of initial activity: Au > Ru ≈ Ir > Pd > Pt ≈ Rh. It is possible that some of the observed differences in activity may be attributed to differences in dispersion. We have previously shown [6] that 1 wt% Au/carbon catalysts have an average Au nanoparticle size of ∼5 nm and range in size from ∼2 to 30 nm. Ideally, it would be best to plot the data in terms of rate of

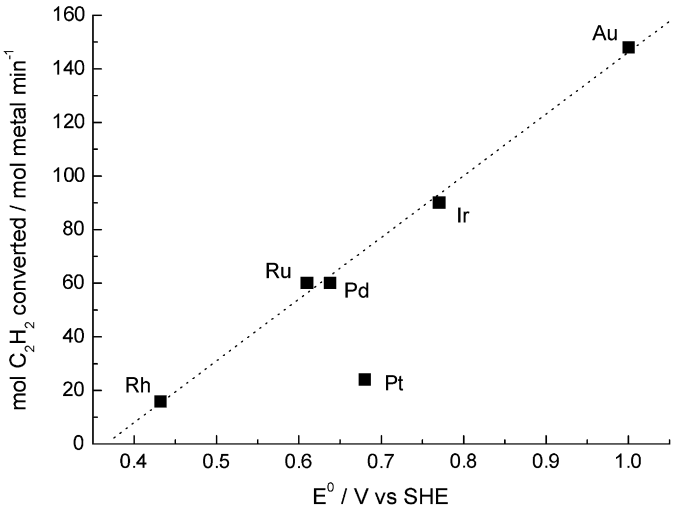


**Fig. 2.** Correlation between initial acetylene conversion versus the standard electrode potential of the various metals used in this study. Potentials are obtained from the reduction potentials of the following chloride salts $(RhCl_6)^{3-}$, $(RuCl_5)^{2-}$, $PdCl_2$, $(PtCl_6)^{2-}$, $(IrCl_6)^{3-}$, and $(AuCl_4)^-$ to the corresponding metals.

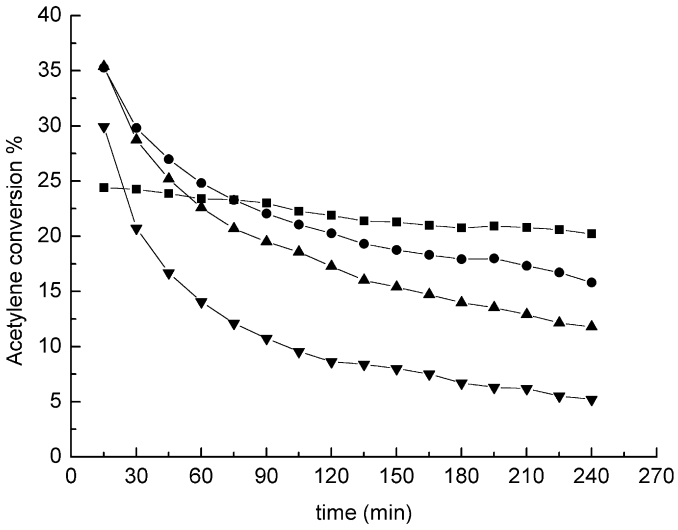


**Fig. 3.** Acetylene conversion for Au and Au/Pd catalysts on carbon for low palladium loading: (■) Au, (●) Au/Pd 99/1, (▲) Au/Pd 95/5, and (▼) Au/Pd 90/10.

conversion per number of exposed surface atoms, rather than as a conversion trend for catalysts composed of equimolar amounts of metal (as shown in Fig. 1). Unfortunately, no chemisorption method for determining Au surface area is available. This is a major problem for gold catalysts that remains to be resolved. However, because the active site for the catalysis involves $Au^{3+}$, such chemisorption methods are not beneficial. Thus, we report the raw experimental data as a conversion trend.

Interestingly, the catalysts displayed different rates of deactivation. Au/C and Ru/C both showed a similar steady slow decline in activity, whereas Pt/C appeared to increase slightly in activity during use. Pd, Ir, and Rh exhibited a more pronounced rapid initial decline in activity. All of these catalysts were able to maintain high selectivity to VCM throughout the entire reaction period, although among the monometallic catalysts, Pd and Ir displayed significant carbonaceous product formation. This was estimated at ca. 3–4% based on $^1H$ NMR characterization of a chloroform extract from a used catalyst, which also demonstrated the presence of hydrogen bonded to conjugated carbons in these deposits, and GC-MS analysis confirmed the presence of Cl. In comparison, the other metals were only slightly affected by carbonaceous product formation.

It is remarkable that it is possible to correlate the initial activity of the catalyst with the standard electrode potential of the metal (Fig. 2). These data fully confirm previous investigations for the hydrochlorination of acetylene, which were based on the suggestion that the reaction was a two-electron process [1]. This proposal has been supported by a recent study of the reaction mechanism [6]. The experimental data in Fig. 2 show a linear correlation with the standard electrode potential; in this case we used the data for the chlorides, which, with the exception of Pt, have initial oxidation state II or III, and considered the reduction $M^{n+}$ to $M^0$. For Pt, which has an initial oxidation state of IV, we used the reduction $Pt^{4+}$ to $Pt^{2+}$ because the reaction is a two-electron process, and reduction to the metal is unlikely. However, it is notable that the initial activity for platinum was much lower than that expected from the correlation, possibly due to the very rapid deactivation of this catalyst. It also should be noted that platinum has a low propensity to form complexes with alkynes but has a high dehydrochlorination activity, leading to a rapid loss of activity. Because we used the data for the chlorides rather than the metals, Fig. 2 represents an extension of our earlier studies in which the correlation was first observed [1]. We discuss the nature of this correlation later in the paper.

### 3.2. Au/Pd on carbon catalysts

#### 3.2.1. Promotion of initial activity by addition of Pd to Au/C catalysts

Catalysts composed of gold and palladium on carbon were prepared at loadings of 0, 1, 5, 10, 20, 50, and 100% Pd atomic fraction (remainder Au) to achieve a total metal loading of 1 wt%, as determined by AAS, with $HAuCl_4{\cdot}xH_2O$ as the precursor for gold and $PdCl_2$ as the precursor for palladium. The catalysts were prepared using co-impregnation of the metals in *aqua regia* solution using an incipient wetness technique. This is the same route used to prepare the Au-only catalysts and is known to be the most effective preparation method [2–6]. We used this impregnation method so as to allow direct comparison of the activity of the bimetallic catalysts with that of the Au-only materials, even though it is not at first glance an optimal procedure for preparing bimetallic catalysts. However, we have recently shown, using STEM–XEDS analysis, [19,20] that this methodology can indeed yield homogeneous alloy nanoparticles for Au–Pd catalysts supported on carbon, and thus we consider it a suitable method for determining whether the addition of a second metal can improve catalyst performance for the hydrochlorination of acetylene. We used this method to prepare of all the catalysts selected for this study. Fig. 3 summarizes the effect of time on stream on activity for this systematic series of Au–Pd bimetallic catalysts. ADF imaging experiments have confirmed that the introduction of low amounts of Pd affected nanoparticle dispersion only slightly, with the average particle size reduced from 4.8 nm in pure Au/C catalysts to 3.4 nm in the Au–Pd/C sample (Fig. 4). Detailed STEM analysis (see later) showed that homogeneous alloys were formed and that no Pd-only particles were generated. At short reaction times, the addition of low levels of Pd ($\leqslant$10 at%) to Au/C led to enhanced activity, but this advantageous effect was rapidly lost.

#### 3.2.2. Characterization of Au/Pd catalysts

Fig. 5 shows TPR results (10% $H_2$ in Ar flow, 50 mL $min^{-1}$; 10 °C $min^{-1}$; final temperature 300 °C held for 1 h) for the fresh catalysts. The Pd-only catalyst reduced at 186 °C, very close to the reaction temperature of the hydrochlorination reaction. In comparison, the Au/C material reduced at a considerably higher temperature (228 °C). For the mixed Au–Pd catalysts, only one reduction peak was observed and the temperature at which reduction occurred increased systematically with increasing gold content. This suggests that a homogeneous alloy of Au–Pd was being formed. This proposition was subsequently confirmed through a detailed

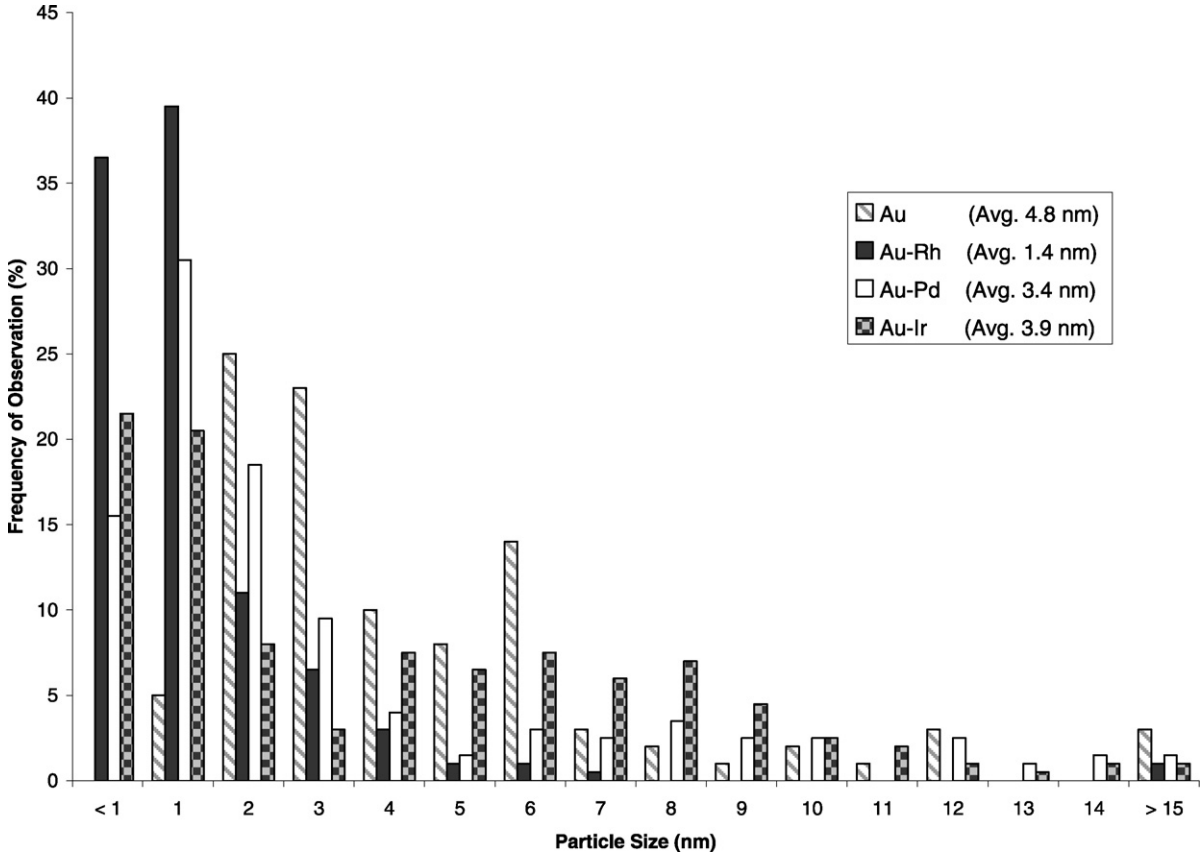


**Fig. 4.** Particle size distributions of Au/C and Au–M/C bimetallic catalysts for hydrochlorination of acetylene (M = Rh, Pd, and Ir). Pure-Au catalyst analyzed using bright-field TEM imaging with 200 kV JEOL 2000 FX TEM w/$LaB_6$ filament; Bimetallic catalysts analyzed using STEM–HAADF imaging with 300 kV, aberration-corrected FEI Titan 80–300 TEM/STEM (FEG); 200 particles measured for bimetallic samples, 100 for the pure-Au/C catalyst.

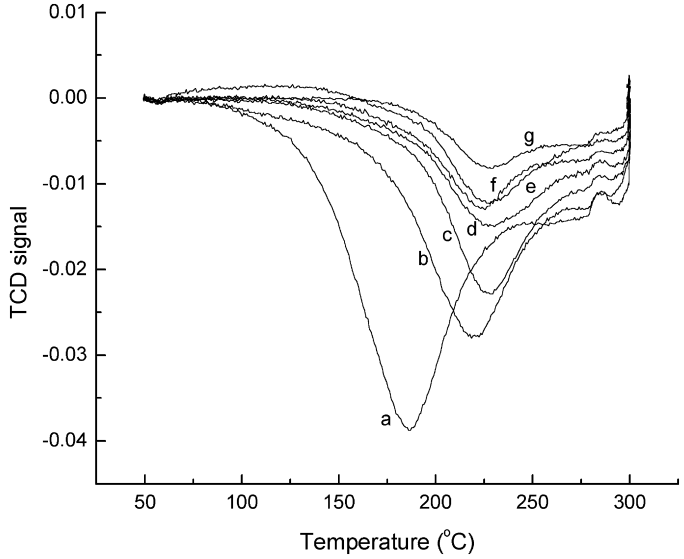


**Fig. 5.** TPR profile for Au, Pd and Au/Pd on carbon catalysts: (a) Pd, (b) Au/Pd 50/50, (c) Au/Pd 80/20, (d) Au/Pd 90/10, (e) Au/Pd 95/5, (f) Au/Pd 99/1, and (g) Au.

STEM–XEDS analysis for the Au:Pd 95:5 catalyst (Fig. 6). It should be noted that the investigation of catalysts with such low concentrations of total metal (1 wt%) to determine whether a minor component is alloyed is a particularly challenging task; we achieved it in the present case by acquiring XEDS spectrum images and processing the data via multivariate statistical analysis [15] (MSA). MSA is a group of processing techniques that can be used to identify specific features and to reduce random noise components in the large STEM–XEDS data sets in a statistical manner. The MSA algorithm performs a data-smoothing calculation by portioning the XEDS data using a probability density function. It was recently shown to be a particularly useful analysis tool for identifying core–shell morphologies in Au–Pd nanoparticles [14,16,17]. Specifically, in the present case, the effect of this processing was to reveal the spectral components of the minor alloying elements by reducing the inherent noise in the data set. For compositional analysis, spectra were summed from a $5 \times 5$ (i.e., 25) pixel area corresponding to the metal particle and the support-only regions indicated by boxes in the STEM–ADF image (Fig. 6a). The emphasis of these studies was on determining the composition of the nanoparticles, rather than focusing on the particle size distribution; nonetheless, a broad distribution of 2- to 15-nm particles was seen in the Au–Pd catalyst. As shown in Fig. 6b, it is clear, within the experimental error limits of standardless k-factor analysis, that the nanoparticles contained Au and Pd at a ratio consistent with the 95 at% Au:5 at% Pd nominal composition. The Si signal originated as a fluorescence artifact of the Si(Li) XEDS detector. Conversely, similar data summed from 25 spectra obtained from the C substrate–only region (Fig. 6c) showed no evidence of Au or Pd, although clearly some residual Cl from the chloride precursor materials remained.

### 3.2.3. Deactivation processes for Au/Pd on carbon catalysts

The VCM selectivity of the Au/C catalyst was almost 100%, and only trace amounts of other products (e.g., dichloroethane) were detected. This was not the case for the Au/Pd catalysts, however, for which the initial selectivity to VCM decreased with increasing Pd content (Fig. 7) and continued to decrease further with increased time on stream. The surface areas of all of the fresh catalysts were very similar (i.e., 500 $m^2\,g^{-1}$), whereas after use they

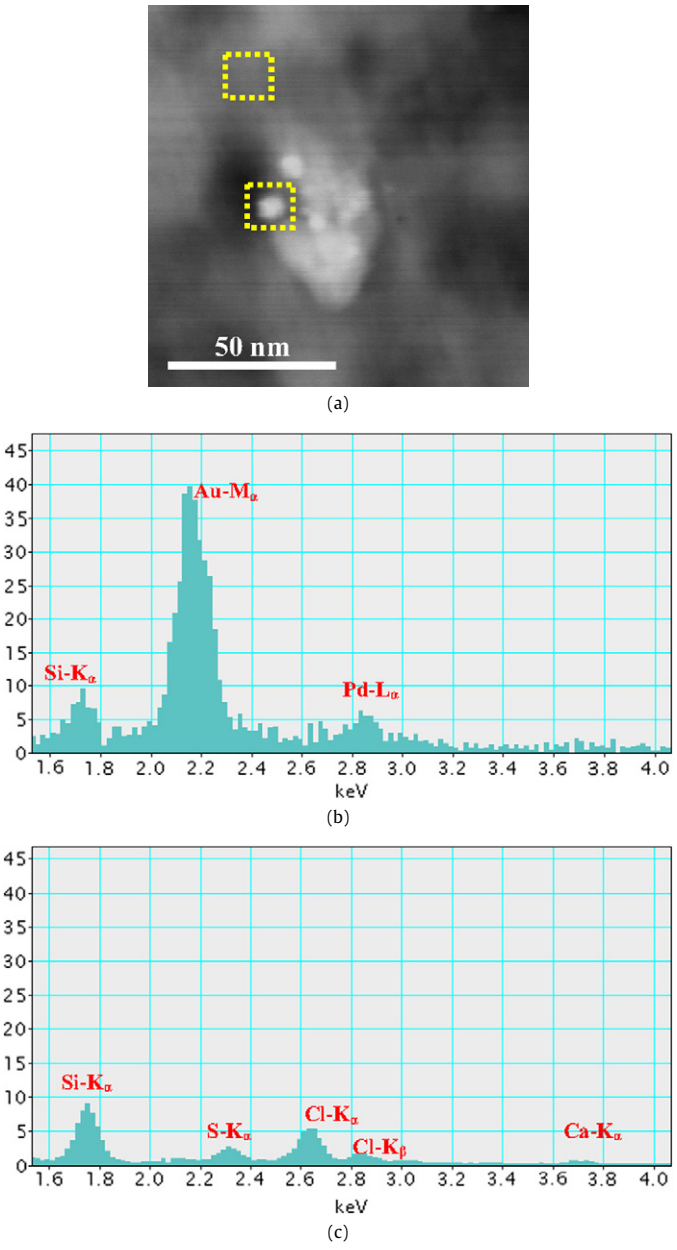


**Fig. 6.** (a) STEM–ADF image of 1 wt% metal (95Au–5Pd)/carbon with the areas indicated from which 5 × 5 XEDS spectra were subsequently summed, (b) XEDS spectrum of the metal particle after MSA, (c) XEDS spectrum of the support after MSA.

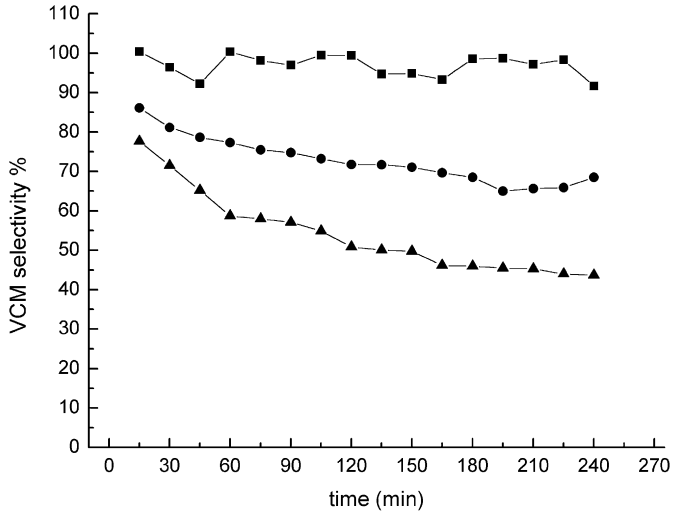


**Fig. 7.** Selectivity as a function of time on-line for the hydrochlorination reaction for the Au–Pd/C catalysts under standard reaction conditions: (■) Au, (●) Au/Pd 99/1, and (▲) Au/Pd 95/5.

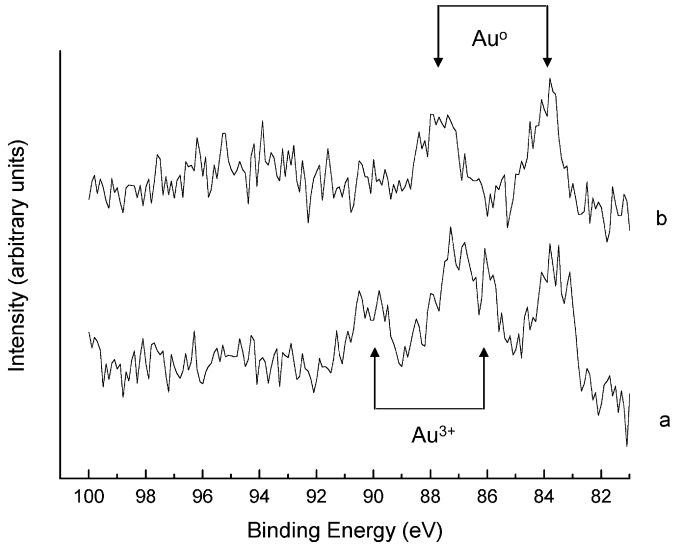


**Fig. 8.** XPS analysis of 1 wt% Au/Pd 95/5 on carbon catalyst; Au 4f peaks (a) before and (b) after reaction. The spectra are relatively noisy due to the low total loading of metal present.

were substantially decreased (Au/C, 460 $m^2 g^{-1}$; 95 at% Au–5 at% Pd/C, 270 $m^2 g^{-1}$; Pd/C, 90 $m^2 g^{-1}$). This effect was particularly marked in the presence of greater amounts of Pd was present. Pd is a known catalyst of dehydrochlorination reactions, and thus the deactivation observed with the addition of Pd to Au/C can be anticipated to be due, at least in part, to oligomer formation, which also could result from a side reaction of alkyne oligomerization catalyzed by the second metal. However, XPS of the fresh and used 95 at% Au–5 at% Pd/C catalysts showed that deactivation was also due to reduction of $Au^{3+}$ species (Fig. 8). Moreover, in separate experiments, we demonstrated that the change in the photoelectron spectra was not simply due to heating at 180 °C, but also required the additional presence of the $C_2H_2$/HCl in the reactant stream. Nevertheless, it is significant that an *initial* promotional effect from the addition of Pd to Au has been observed. But this effect occurs along with a loss in selectivity to VCM, and thus we consider that the enhanced activity may be related to oligomer formation. This is consistent with our previous studies [4] in which we found that one of the key mechanisms of catalyst deactivation in the acetylene hydrochlorination reaction was coke deposition due to the nondesorption of reactants and products as well as polymerization of the vinyl chloride. This was confirmed using a detailed TGA investigation, because the determination of coke levels on a catalyst comprising 99% carbon is very challenging.

### 3.3. Au/Ir on carbon catalysts

We prepared a systematic series of Au/C, Ir/C, and Au–Ir/C catalysts with a total metal content of 1 wt%, as confirmed by AAS, using $IrCl_3 \cdot 3H_2O$ as the iridium precursor. These were evaluated for the hydrochlorination of acetylene. The addition of low levels of Ir (1 and 5 at%) produced an enhancement in activity (Figs. 9a and 9b) similar to that observed with Pd (Fig. 3); however, the loss of selectivity to VCM was observed only at the 1 at% Ir loading level, suggesting that oligomer formation was occurring in this case. The addition of higher levels of Ir also led to an enhancement

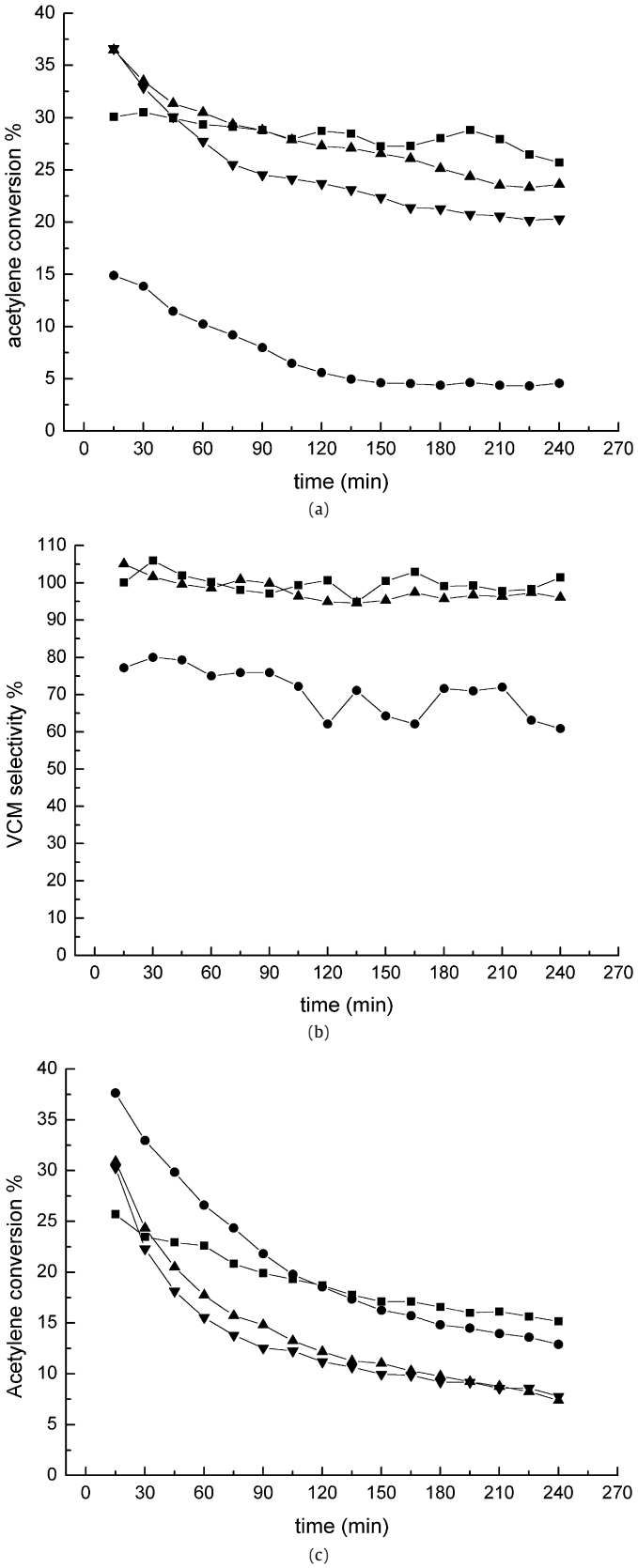


**Fig. 9.** Hydrochlorination of acetylene over Ir–Au/C catalysts (a) (■) acetylene conversion for Au, (●) Ir, (▲) Au/Ir 99/1, and (▼) Au/Ir 95/5 on carbon; (b) VCM selectivity for (■) Au, (●) Au/Ir 99/1, and (▲) Au/Ir 95/5 on carbon for hydrochlorination reaction of acetylene; (c) Au/Ir catalysts on carbon with high Ir loading for the hydrochlorination reaction of acetylene on carbon: (▼) Au/Ir 20/80, (▲) Au/Ir 50/50, (●) Au/Ir 80/20, and (■) Au.

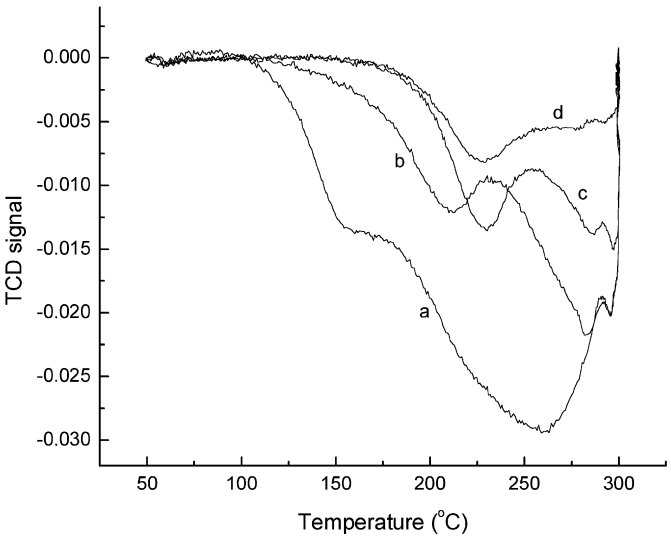


**Fig. 10.** TPR profiles for Au/Ir catalysts: (a) Ir, (b) Au/Ir 95/5, (c) Au/Ir 99/1, and (d) Au on carbon.

in initial activity (Fig. 9c), which differs significantly from the behavior noted for the Au–Pd/C catalysts.

XPS analyses of fresh and used Au–Ir catalysts showed similar features to those of the Au–Pd catalysts presented in Fig. 8, with the loss in activity associated with reduction of $Au^{3+}$ from the catalyst [6,7]. TPR of the fresh Au–Ir catalysts (Fig. 10) showed that the addition of >1 at% Ir to Au led to two reduction features, suggesting that a simple homogeneous alloy was not formed above this dopant concentration. The Au–Ir catalyst contained metal particles of slightly smaller average size (3.9 nm) than that of the pure Au/C catalyst (Fig. 4). A methodology similar to that used to examine the Au–Pd STEM–XEDS spectrum imaging data was used to analyze the Au and Ir spatial distributions in this catalyst. The Au–Ir catalyst had a similar broad particle size distribution as the Au–Pd catalyst, with particles ranging in size from 2 to 15 nm. As denoted by the boxes in the ADF image shown in Fig. 11a, data were again extracted from $5 \times 5$ pixel sets both "on" and "off" the metal particle. The corresponding sum spectra from these areas (Figs. 11b and 11c, respectively) indicate that the Ir did not alloy strongly with Au, but instead remained widely dispersed on the carbon support. This is evident from the absence of Ir$M_\alpha$ signal in the spectra obtained from the metal particle (Fig. 11b). But the Ir$M_\alpha$ signal was just about detectable at 1.978 keV in the spectrum extracted from the support-only area (Fig. 11c); therefore, even with the very small overall amount of Ir metal present in this sample, the combination of aberration-corrected STEM–XEDS spectrum imaging and MSA processing revealed the spatial distribution of Ir in this catalyst.

We tested catalysts containing higher Ir loadings (Fig. 9c) and found that materials containing up to 20 at% Ir (within the 1 wt% total loading) gave enhanced initial activity compared with undoped Au/C. This is in direct contrast to the results observed with Pd; this enhancement was rather short-lived, however. Furthermore, Ir exerted a promotional effect at high loadings, although the deactivation rate was considerably higher than at low Ir loadings.

### 3.4. Au/Rh on carbon catalysts

Catalysts containing 0, 5, 10, 20, 50, 80, and 100% Rh atomic fraction (remainder Au) were prepared, for a total loading of 1 wt% metal, as confirmed by AAS, using $HAuCl_4 \cdot xH_2O$ and $RhCl_3 \cdot 3H_2O$. It is immediately evident that the general trend in catalytic behavior (Fig. 12) was now quite different from that observed with

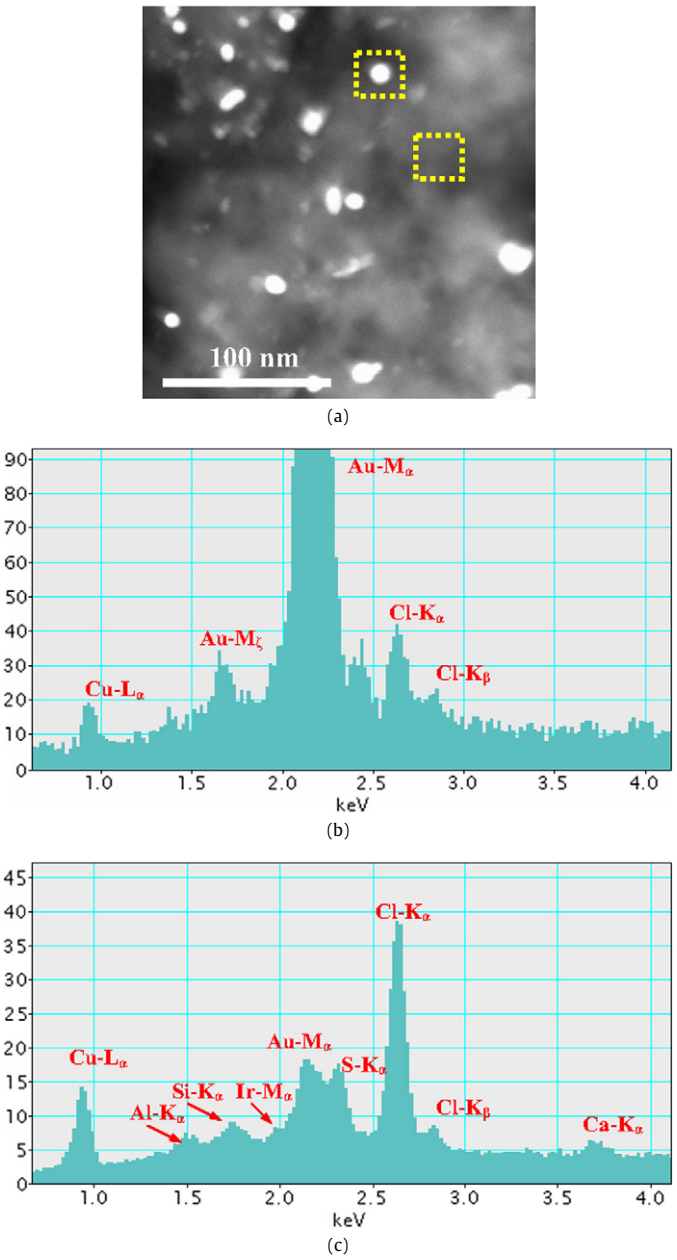


**Fig. 11.** (a) STEM–ADF image of 1 wt% metal (80 Au–20 Ir)/carbon with the areas indicated from which 5 × 5 XEDS spectra were subsequently summed, (b) XEDS spectrum of the metal particle after MSA, (c) XEDS spectrum of the support after MSA.

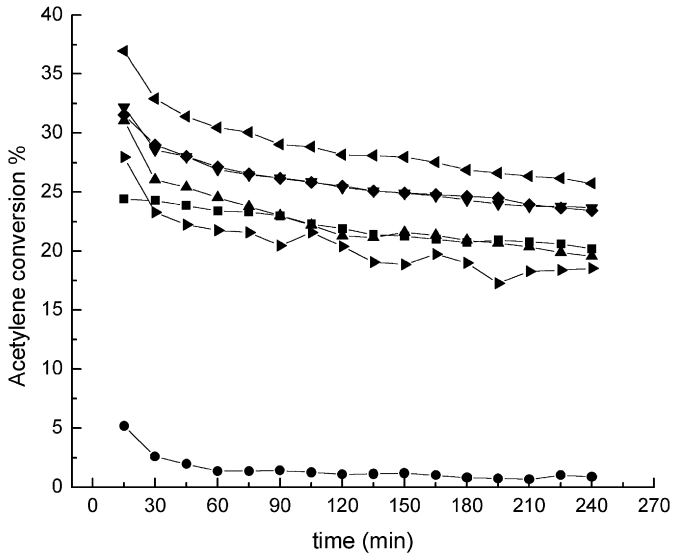


**Fig. 12.** Acetylene conversion for Au/Rh catalysts: (●) Rh, (►) Au/Rh 20/80, (◄) Au/Rh 50/50, (◆) Au/Rh 80/20, (▼) Au/Rh 90/10, (▲) Au/Rh 95/5, and (■) Au.

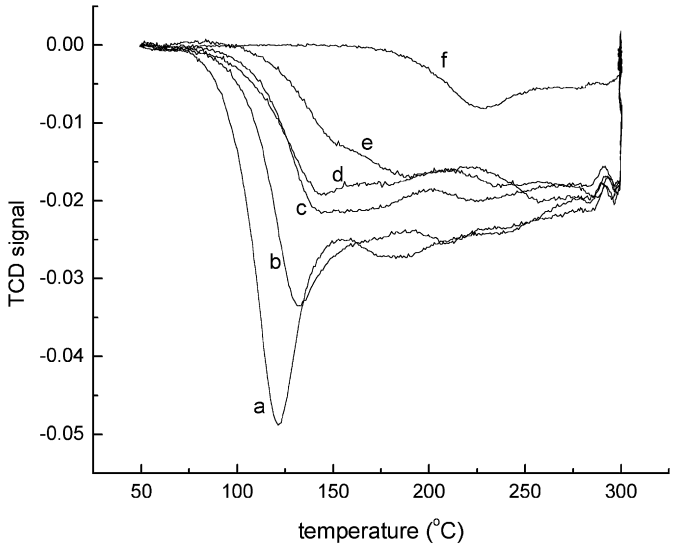


**Fig. 13.** TPR profiles of Au/Rh catalysts: (a) Rh, (b) Au/Rh 50/50, (c) Au/Rh 80/20, (d) Au/Rh 90/10, (e) Au/Rh 95/5, and (f) Au on carbon.

Au/Pd (Fig. 7) or Au/Ir (Fig. 9). The first observation is that a higher conversion was obtained for Au/Rh catalysts with Rh content up to 50%. Furthermore, this significantly enhanced activity was seen not only in the initial stages, but for the entire time on stream. This is also reflected in the selectivity, which was always >95–98%, similar to that observed for the Au-only catalysts. XPS analyses of fresh and used catalysts showed similar features to those of the Au–Pd catalysts (Fig. 8), with the decrease in activity once again associated with reduction of $Au^{3+}$ in the catalyst [6,7]. But TPR of the Au–Rh/C catalysts (Fig. 13) showed significant differences from the Au–Pd catalysts (Fig. 5). In particular, all of the Rh-containing catalysts exhibited three reduction features even at low Rh loading, indicating that little significant alloy formation occurred in these catalysts.

The Au–Rh catalyst contained metal particles of smaller average size (1.4 nm) compared with those of the pure Au/C, Au–Pd/C, and Au–Ir/C samples, but a few larger particles (20–30 nm) also were found (Fig. 4). Detailed STEM–XEDS analysis of the 90 at% Au:10 at% Rh (1 wt% total metal loading) catalyst was performed as described above; the data are presented in Fig. 14. Interpretation of the spectral data obtained from this particular sample is complicated by the presence of Cl in both of the metal precursors ($HAuCl_4$ and $RhCl_3$) used during impregnation. This is because the Cl$K_\alpha$ peak overlaps the Rh$L_\alpha$ peak (2.62 and 2.69 keV, respectively) and also because some residual Cl was no doubt retained in the sample, making it very difficult to conclusively determine which of these two elements gave rise to the observed spectral features. The Cl$K_\beta$ and Rh$L_\beta$ peaks overlapped even more significantly (2.82 and 2.83 keV, respectively); thus, even examining these more minor spectral features does not particularly aid our interpretation of the data. As shown in Fig. 14, the XEDS spectra extracted from a 10-nm metal particle (b) in the Au–Rh catalyst demonstrates the presence of Au with only a very small feature (indicated by the arrow), barely distinguishable from the noise, at the energy expected for Cl and Rh. In contrast, the sum spectrum extracted from the support area (c) shows a very definite peak at

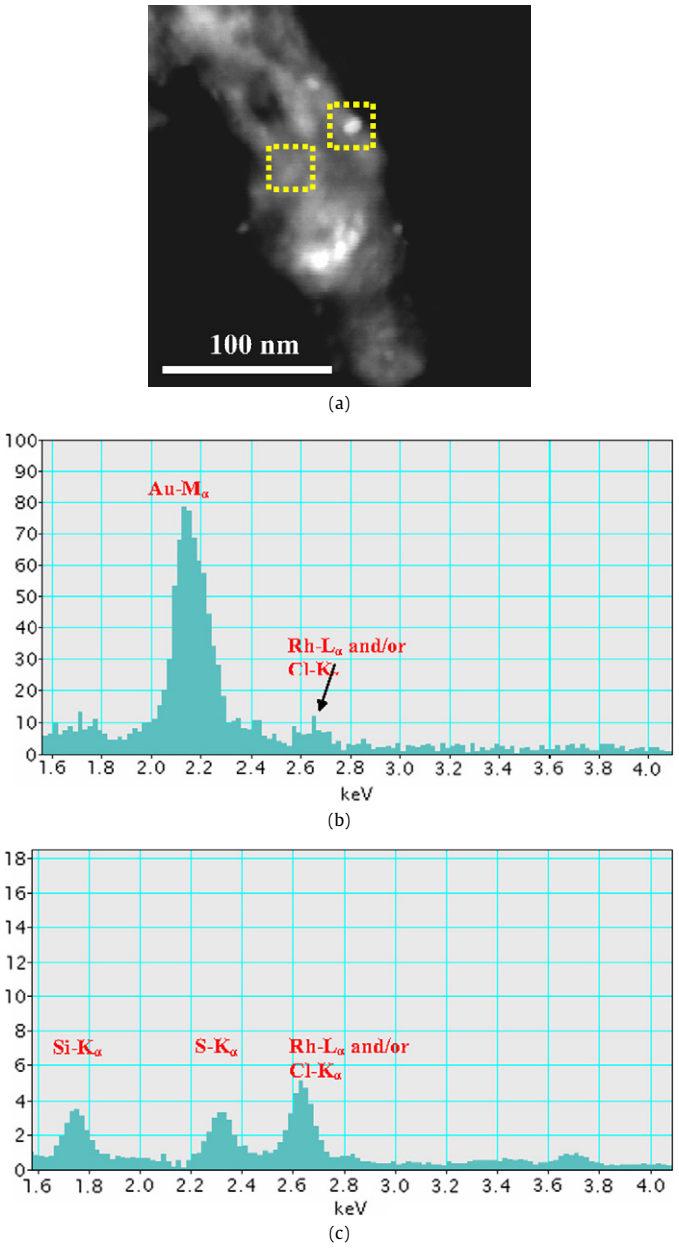


**Fig. 14.** (a) STEM–ADF image of 1 wt% (90 Au–10 Rh)/carbon with the areas indicated from which 5 × 5 XEDS spectra were subsequently summed, (b) XEDS spectrum of the metal particle after MSA, (c) XEDS spectrum of the support after MSA.

2.68 keV but no discernible Au signal. Therefore, it is highly probable that the metal particles in the Au–Rh system had a very poor tendency to alloy, and thus most (if not all) of the Rh remained dispersed on the carbon support.

### 3.5. Au/Pt on carbon

We prepared a systematic series of Au/C, Pt/C, and Au–Pt/C catalysts with a total metal content of 1 wt%, as confirmed by AAS, using $H_2PtCl_6$ as the platinum precursor. These were subsequently evaluated for the hydrochlorination of acetylene. The addition of Pt to Au produced an enhancement of initial activity for catalysts containing up to 5 at% Pt but not for those with higher Pt concentrations (see Fig. S2 in Supplementary material). Thus, the Au/Pt catalysts behaved similarly to the Au/Pd catalysts. XPS analysis of fresh and used catalysts showed similar features to those of the Au–Pd catalysts (Fig. 8), and once again we consider the loss in activity to be associated with reduction of $Au^{3+}$ species in the catalyst [6,7].

### 3.6. Au/Ru on carbon

We prepared a series of Au/C, Ru/C, and Au–Ru/C catalysts with a total metal content of 1 wt%, as confirmed by AAS, using $RuCl_3 \cdot H_2O$ as the rhodium precursor, and evaluated them for the hydrochlorination of acetylene. At best, we found only the activity and selectivity expected for the gold-only catalysts (see Fig. S3 in Supplementary material).

### 3.7. Comments on the nature of the bimetallic catalysts on hydrochlorination activity

The bimetallic catalysts that we examined exhibited a number of interesting features. First, the XPS analysis of fresh and used catalysts was consistent with previous observations of monometallic Au/C catalysts, namely a substantial reduction of $Au^{3+}$ during use, which is associated with catalyst deactivation [6,7]. We propose that the activity trends of these catalysts can be explained in terms of the relative solubility of the metal additives in Au [21–23] and the known interactions of the metallic species with chlorinated hydrocarbons.

The Au–Pd/C and Au–Pt/C catalysts showed very similar catalytic effects; at low levels of Pd and Pt (<5 at%), there was an enhancement in initial activity, but this was associated with loss in selectivity. In addition, all of the Au–Pd/C and Au–Pt/C catalysts exhibited very rapid deactivation compared with undoped Au/C at all of the doping levels investigated. Pd and Pt were both completely soluble in Au across the entire range of compositions [21–23]; thus, it can be reasonably expected that alloy nanoparticles were formed for these bimetallic catalyst systems. This in fact was confirmed by TPR and STEM–XEDS analysis of the Au–Pd/C catalysts (Figs. 5 and 6). But both Pd and Pt are very effective dehydrochlorination catalysts, and as such, they tended to react with the VCM, leading to coke deposition on the surface and thereby decreasing the VCM selectivity and lifetime. Therefore, the short-lived enhancement in activity was most likely related to oligomerization of acetylene initiated by the presence of Pd or Pt in the alloys reacting with VCM [24–26].

Pure Ir showed similar behavior to that of the 1 at% Ir:99 at% Au-doped sample (Figs. 9a and 9b). According to equilibrium binary-phase diagrams, Ir is soluble in Au at levels up to 2 at% [21–23] and so the 1 at% Ir–Au material can be expected to be a very dilute alloy that acts similar to the Pd- and Pt-doped catalysts. At higher Ir levels, no effect on selectivity was seen, along with an enhancement of activity, which we ascribe to enhanced dispersion of the Au, because the additional Ir is insoluble in Au in these compositions. A similar effect was observed for Au–Rh/C catalysts. Binary-phase diagrams also suggest that Rh had very limited solubility in Au (ca. <1%), slightly lower than that of Ir [21–23]; the lack of significant alloying is consistent with our STEM–XEDS studies (Fig. 13). However, at present, we cannot conclusively detect very dilute alloys with this technique. The Au–Rh/C catalysts all showed VCM selectivities similar to those of undoped Au/C catalysts with no marked deactivation. In view of this finding, we propose that the increased activity for the Au–Rh catalysts could be due to two effects: a slightly enhanced dispersion of gold and the inability to form homogeneous alloy particles containing substantial quantities of Au and Rh [21–23]. However, in principle, very dilute alloy particles in which the Rh concentration is below the solubility limit of Rh in Au could be present, as could Rh species containing trace amounts of Au. Given the analytical sensitivity of the STEM–XEDS technique, discerning whether this is present in the current catalysts is not a trivial task. In contrast, Ru is virtually

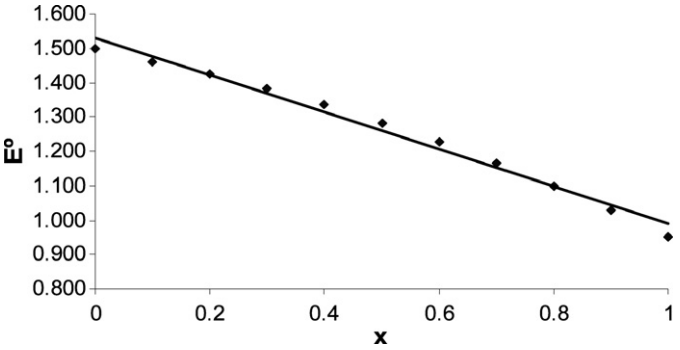


**Fig. 15.** Standard electrode reduction potential vs palladium mole fraction in a PdAu alloy. For full calculation, see supplementary data.

insoluble in Au [21–23], and, consequently, no effects (negative or positive) on catalytic activity from the addition of Ru to Au/C were observed.

To date, our attempts to improve the activity of gold for the hydrochlorination of acetylene by the addition of a second metal have not succeeded. The observation that the monometallic gold catalysts are indeed the best catalysts for this reaction is wholly consistent with the previously reported correlation between catalyst activity and the standard electrode potential [1,3]. Indeed, any dilution of gold by a second metal when present as a homogeneous alloy, as is the case for Au–Pd (Fig. 6) [21–23], will lead to a decrease in the standard electrode potential, which is a linear function of the fraction, *x*, of dopant metal added (see Fig. 15 for the Au–Pd case; full details are given in Supplementary material, Table S2 and Fig. S4).

The correlation with the standard electrode potential merits some additional comments. The original observation of this correlation [1] correctly predicted that $Au^{3+}$ would be the best catalyst for acetylene hydrochlorination. The origin of the correlation likely is related to the interation between the gold catalyst and the reactants. In our earlier mechanistic study, we found that acetylene and HCl interacted with the gold active site to form vinyl chloride and also to restore the nature of the active site. It is possible that the reactivation of the gold site by HCl after desorption of the vinyl chloride product is the crucial step, leading to the observation of this correlation. In addition, is feasible that a similar mechanism operates for all of the materials evaluated as catalysts to date, because all of the reaction data we have obtained agree with this correlation [1,3].

All of the data collected in the present study suggest that improvements in the design of gold-based catalysts for the hydrochlorination of acetylene will need to focus on methods of catalyst preparation that can lead to enhanced gold dispersion and improved stabilization of its higher oxidation state. The correlation of activity with the standard electrode potential confirms that the active species for this reaction is cationic gold $Au^{3+}$. Although no chemisorption methods are available for reliably determining the dispersion of metallic gold, a combination of XPS and TEM can be used to determine the number of surface exposed $Au^{3+}$ species present in a fresh catalyst sample. We have attempted to determine this for a standard 1 wt% Au/C catalyst (full details are given in the supplementary information) and found a TOF of 480 $h^{-1}$ for the initial activity under the standard reaction conditions. Although in principle this approach can be extended to bimetallic systems, this is infeasible at present, because different microscopy techniques are needed to determine the particle size distribution (TEM) and the composition of individual particles (STEM mapping). In addition, we have recently shown that the composition of Au–Pd homogeneous alloy particles supported on carbon is a function of particle size [19]. Therefore, considerably more effort will be required to determine the surface $Au^{3+}$ concentration in mixed-metal systems.

## Acknowledgments

The authors acknowledge the support of the Engineering and Physical Sciences Research Council (EPSRC) of the UK and Johnson Matthey plc (project ATHENA) and the European Union (project AURICAT; contract HPRN-CT-2002-00174). The authors thank Dr. Peter Johnston of Johnson Matthey for detailed discussions and suggestions, as well as the World Gold Council for sponsoring M.C. under the GROW scheme. C.K. and A.H. gratefully acknowledge funding from the National Science Foundation through the following grants: DMR-0079996, DMR-0304738, and DMR-0320906.

## Supplementary material

The online version of this article contains additional supplementary material.

Please visit DOI:10.1016/j.jcat.2008.04.024.

## References

[1] G.J. Hutchings, J. Catal. 96 (1985) 292.
[2] B. Nkosi, N.J. Coville, G.J. Hutchings, J. Chem. Soc. Chem. Commun. (1988) 71.
[3] B. Nkosi, N.J. Coville, G.J. Hutchings, Appl. Catal. 43 (1988) 33.
[4] B. Nkosi, N.J. Coville, G.J. Hutchings, M.D. Adams, J. Friedl, F.E. Wagner, J. Catal. 128 (1991) 366.
[5] B. Nkosi, N.J. Coville, G.J. Hutchings, M.D. Adams, J. Friedl, F.E. Wagner, J. Catal. 128 (1991) 378.
[6] M. Conte, A.F. Carley, C. Heirene, D.J. Willock, P. Johnston, A.A. Herzing, C.J. Kiely, G.J. Hutchings, J. Catal. 250 (2007) 231.
[7] G.J. Hutchings, D.T. Grady, Appl. Catal. 16 (1985) 411.
[8] G.J. Hutchings, D.T. Grady, Appl. Catal. 17 (1985) 155.
[9] G.C. Bond, D.T. Thompson, Catal. Rev. Sci. Eng. 41 (1999) 319.
[10] M. Haruta, Gold Bull. 37 (2004) 27.
[11] A.S.K. Hashmi, Gold Bull. 37 (2004) 51.
[12] A.S.K. Hashmi, G.J. Hutchings, Angew. Chem. Int. Ed. 45 (2006) 7896.
[13] P. Landon, P.J. Collier, A.J. Papworth, C.J. Kiely, G.J. Hutchings, Chem. Commun. (2002) 2058.
[14] D.I. Enache, J.K. Edwards, P. Landon, B. Solsona-Espriu, A.F. Carley, A.A. Herzing, M. Watanabe, C.J. Kiely, D.W. Knight, G.J. Hutchings, Science 311 (2006) 362.
[15] MSAXESP v. 0.11, M. Watanabe, 2005.
[16] P. Trebbia, N. Bonnet, Ultramicroscopy 34 (1990) 165.
[17] M.G. Burke, M. Watanabe, D.B. Williams, J.M. Hyde, J. Mater. Sci. 41 (2006) 4512.
[18] M. Watanabe, D.W. Ackland, A. Burrows, C.J. Kiely, D.B. Williams, O.L. Krivanek, N. Dellby, M.F. Murfitt, Z. Szilagyi, Microscop. Microanal. 12 (2006) 515.
[19] A.A. Herzing, M. Watanabe, J.K. Edwards, M. Conte, Z.-R. Tang, G.J. Hutchings, C.J. Kiely, Faraday Discuss. 138 (2008) 337.
[20] J.K. Edwards, A.F. Carley, A.A. Herzing, C.J. Kiely, G.J. Hutchings, Faraday Discuss. 138 (2008) 225.
[21] M. Hansen, Constitution of Binary Alloys, second ed., McGraw–Hill, New York, 1958.
[22] R.P. Elliott, Constitution of Binary Alloys, First Supplement, McGraw–Hill, New York, 1965.
[23] F.A. Shunk, Constitution of Binary Alloys, Second Supplement, McGraw–Hill, New York, 1969.
[24] A. Aranzabal, J.A. González-Marcos, J.L. Ayastuy, J.R. González-Velasco, Chem. Eng. Sci. 61 (2006) 3564.
[25] D.R. Luebke, L.S. Vadlamannati, V.I. Kovalchuk, J.L. d'Itri, Appl. Catal. B 35 (2002) 211.
[26] S. Ordóñez, F.V. D'ıez, H. Sastre, Appl. Catal. B 31 (2001) 113.